Available online at www.sciencedirect.com
ScienceDirect
Journal of the European Ceramic Society 27 (2007) 1983–1989
www.elsevier.com/locate/jeurceramsoc

Iron-oxide nanoparticles supported on sepiolite as a novel humidity sensor

Antonio Esteban-Cubillo [a], Jean-Marc Tulliani [b], Carlos Pecharromán [a], José S. Moya [a,*]

[a] *Instituto de Ciencia de Materiales de Madrid, CSIC, Cantoblanco, Madrid 28049, Spain*
[b] *Politecnico di Torino, Materials Science Department, Cso. Duca degli Abruzzi, 24, 10129 Turin, Italy*

Received 15 May 2006; received in revised form 24 May 2006; accepted 26 May 2006
Available online 4 August 2006

Abstract

In the present work, a new humidity sensor based on nanostructured hematite deposited by a wet chemical route on a low-cost natural inorganic phylosilicate (sepiolite) powder was obtained. The nanometric character of these particles has been evaluated by X-ray diffraction, thermal gravimetric analysis (TGA) and differential thermal analysis (DTA) and transmission electron microscopy. This material compacted as a pellet by uniaxial pressure with the corresponding interdigitated gold electrodes, was found to be very appropriate to operate as humidity sensor over a wide relative humidity (RH) range (5–98%).

Keyword: Nanocomposite; Surface; Porosity; Sensor; Sepiolite

1. Introduction

The demand for humidity sensors has notably increased during the last decades,[1–4] both for industrial applications (production of paper, fibres, materials for electronics, fabrication of precision instruments) as well as for the end-user market, such as air conditioners, dryers, dehumidificators, microwave ovens, electrical household medical equipment[5] (apparatus for assisted respiration, sterilizers, incubators), and agriculture system (programmed irrigation for water saving, control of the hothouse cultivation); for safety and environmental control systems also the knowledge of relative humidity value is of crucial importance.[6]

Among the different ceramic systems, the type of conduction might be electronic or ionic.[7–10] In any case, a matrix with a high specific surface area is required to support the sensing component as for example, infiltrated silica.[11] In this sense, the use of nanostructured materials improves the sensibility of the different sensors because they present a higher specific surface area.[12]

Among the proton conducting materials, a special role is played by such iron oxides as α-Fe_2O_3 and Fe_3O_4, as a consequence of their low cost and the possibility to modify their functional properties by means of proper doping, or by mixing oxides having different oxidation states. The humidity sensing mechanism of iron oxide was early studied in the decade of 1970.[13] Recently massive devices,[14] sensors based either on thin films deposited by a liquid phase[14,15] or on thick screen-printed films[16] have been proposed in the literature and also doped Fe_3O_4 based-colloidal films.

Porous ceramics have been widely investigated as humidity sensors because of their structures with open pores which tend to favour water and gases adsorption and condensation. Electrical properties are largely related to the porosity and the pore size distribution of the open pores.[17]

The objective of the present work is to prepare hematite (α-Fe_2O_3) nanoparticles supported on sepiolite ($Si_{12}O_{30}Mg_8(OH,F)_4(H_2O)_4{\cdot}8H_2O$)[18] in order to operate over a wide range of relative humidity (RH) by a simple low cost procedure. Moreover, a large quantity of this material can be obtained in a straightforward manner and can be easily scaled-up for industrial applications. Additionally, the fact that these nanoparticles are supported on an inert matrix makes all the manipulation process easier.

2. Experimental methods

Iron oxide nanoparticles embedded into sepiolite were obtained by a wet chemical route. The starting sepiolite powder (TOLSA, Spain), obtained from mineral ores, was purified

* Corresponding author. Tel.: +34 913349083; fax: +34 913349083.
E-mail address: jsmoya@icmm.csic.es (J.S. Moya).

0955-2219/$ – see front matter © 2006 Elsevier Ltd. All rights reserved.
doi:10.1016/j.jeurceramsoc.2006.05.108

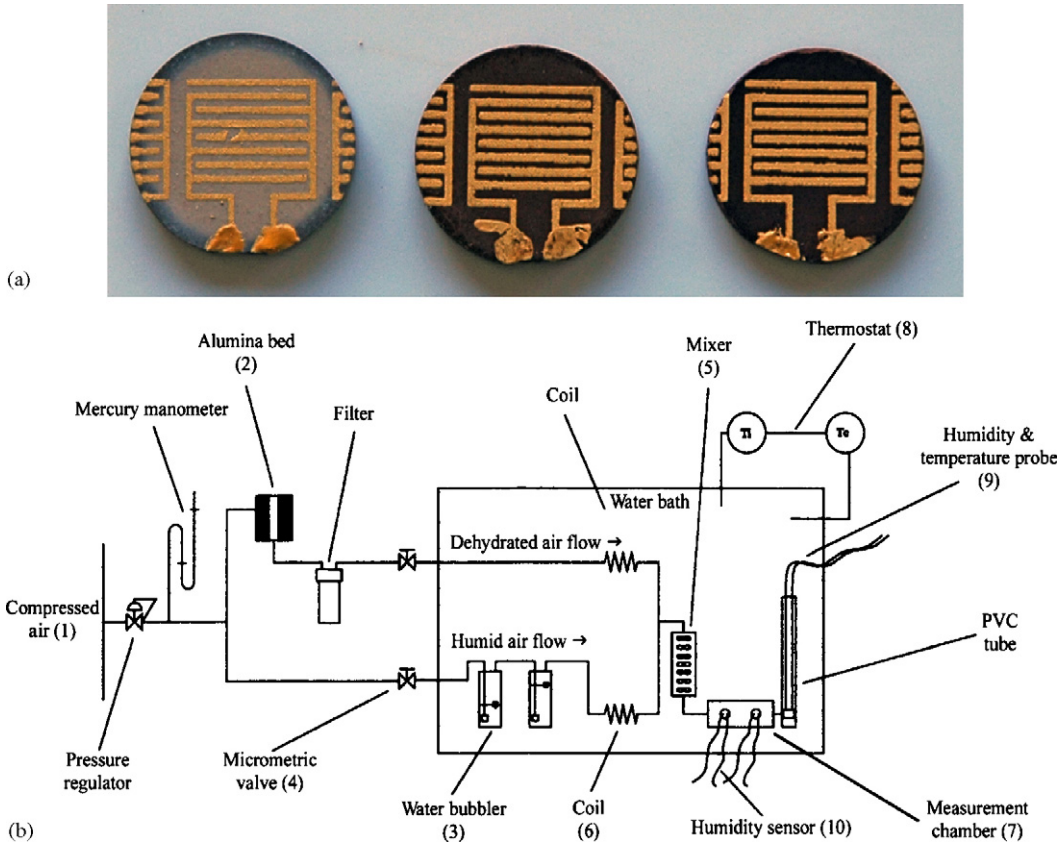

Fig. 1. (a) From left to right, pure sepiolite, S10 and S47 pellets, respectively, with integrated electrodes and (b) scheme of the laboratory apparatus for sensors testing.

and micronized by a wet process with a particle size below 1 μm. 7.5 g of the resulting sepiolite powder was dispersed at 10 wt.% concentration in water using high shear mixing. This suspension was gradually acidified, by HNO_3, to reach a final pH value of pH 2. Afterwards, this sepiolite suspension was mixed with variable amounts of aqueous solutions of $Fe(NO_3)_2{\cdot}7H_2O$ (0.75 and 3.5 g) so that the final iron content on sepiolite was 10 and 47 wt.% (S10 and S47, respectively). Thereafter, the pH of the dispersion was adjusted with NaOH to stabilize the pH of the suspension at pH 8 in order to precipitate all the iron species. Then, the dispersion was vacuum filtered and washed with water. The chemical analysis of this solution (determined by inductively coupled plasma atomic emission spectrometry, ICP-AES, using a Thermo Jarrell Ash model Iris Advantage spectrophotometer) detected large concentrations of Mg^{2+}, but a nearly total absence of the iron cations. The filtration cake was dried at 150 °C overnight.

X-ray diffraction patterns were recorded in a D8 Bruker diffractometer using Cu Kα radiation. The weight loss and structural changes during thermal decomposition of samples were determined by thermal gravimetric analysis (TGA) and differential thermal analysis (DTA) in a Stanton Mod. STA 781. Transmission electron microscopy (TEM) images were taken by a JEOL microscope model FXII operating at 200 kV.

The BET (Brunauer–Emmet–Teller) specific surface area of the different samples was determined using FlowSorb II 2300 equipment.

Powder pellet sensors were prepared by pressing iron/sepiolite powders under a uniaxial pressure of 300 MPa, to prevent any shrinkage during the thermal treatment after metallic electrodes deposition and also to slightly increase their mechanical properties. Interdigitated gold electrodes (ESL 8835, 520C, from Electro-Science, King of Prussia, PA, USA) were screen printed prior to firing at 520 °C for 15 min (Fig. 1a) following the ink manufacturer's recommendations. Resistance measurement were performed in a controlled humidity chamber, in which the relative humidity could be varied between 5% and 98% (Fig. 1b) keeping the temperature of the measuring environment constant at 19 or 40 °C. In this chamber, compressed air (1) was separated into two fluxes: one was dehydrated over a chromatography alumina bed (2) while the second one was directed through two water bubblers (3), generating, respectively, a dry and a humid flow. Two precision microvalves (4) allowed to recombine the two fluxes into one by means of a mixer (5) and to adjust the RH content while keeping constant the testing conditions: a flow rate of 0.1 l/s at 1 m/s. Then, the relative humidity was not increased in a continuous mode but was varied by steps. The bubblers, the coils (6) through which the two fluxes passed in, the mixer and the measurement chamber (7) were immersed in a thermostated water bath (8), which in this case operated at 19 or 40 °C. A commercial, humidity and temperature probe (9) was used as reference for temperature and RH values (Delta Ohm DO9406, accuracy: ±2.5% in the 5–90% RH range). Each tested sensor

(10) was alimented by an external alternating voltage ($V = 3.6$ V at the rate of 1 kHz) and then constituted a variable resistance of this electrical circuit. A 2000 Keithley digital multimeter was used to measure the tension V_{DC} at the output of the circuit. The sensor resistance was determined by substituting them, in the circuit, by known resistances and then plotting a calibrating curve $R = f(V_{DC})$. Two sensors of each composition and thermal treatment temperature were tested at each time.[19]

It should be noted that this material is stable at an air atmosphere for long term periods. In fact, the samples remained unchanged after 1 year.

3. Result and discussion

Iron oxide nanoparticles supported on a sepiolite matrix were obtained by mean of a weak acid attack (pH 2) with HNO_3 (3 M).[20–22] This process leaches the magnesium cations located at the surface of the phylosilicate particles according to

$$Mg_8Si_{12}O_{30}(OH)_4(H_2O)_4 \cdot 8H_2O + xH^+ \rightleftarrows Mg_{8-x}H_{2x}Si_{12}O_{30}(OH)_4(H_2O)_4 \cdot 8H_2O + xMg^{2+}$$

Subsequently, a water solution of iron is added to the suspension and after some time to homogenize the suspension (1 h), the pH is raised by the addition of NaOH. According to the potential-pH equilibria diagrams,[23] iron cation is not stable into the aqueous solution from pH 3 while magnesium cation remains into the solution up to pH 8. During this process, a fraction of iron cations occupy on the sepiolite magnesium vacancies forming a variety of stable iron sepiolite. This material has been found in the nature, and is called ferricsepiolite or xylotile.[24] The amount of adsorbed Fe^{3+} ions in sepiolite balances the dissolved Mg^{2+} ions:

$$Mg_{8-x}H_{2x}Si_{12}O_{30}(OH)_4(H_2O)_4 \cdot 8H_2O + (3x/2)Fe^{3+} \rightleftarrows Mg_{8-3x/2}Fe_{3x/2}Si_{12}O_{30}(OH)_4(H_2O)_4 \cdot 8H_2O + 2xH^+$$

Once the surface vacancies are fully occupied and if the metal concentration is high enough, the excess of iron cations precipitate on the iron cations located at the sepiolite surface as nanometric oxides (particles below 10 nm).

Fig. 2 includes the X-ray diffraction patterns of sepiolite and sepiolite/iron oxide S10 and S47. In the case of S10 sample, the diffractogram seems to be identical to that of sepiolite, indicating that a fraction of iron cations substitutes magnesium to form an iron sepiolite. In this case, although no iron oxide phase was detected by XRD, it is not possible to discard its presence, especially if its particle size is very small (<10 nm), as it can be observed in Fig. 3a. Conversely, in the S47 sample, XRD peaks corresponding to precipitated α-Fe_2O_3 are clearly visible (Fig. 2c).

The thermal evolution in air of the S10 and S47 samples presents the loss of zeolitic water and a double dehydration process corresponding to the loss of two pairs of coordination water molecules (Fig. 4). In fact, sepiolite presents two types of water molecules in the crystalline channels, zeolitic water, asso-

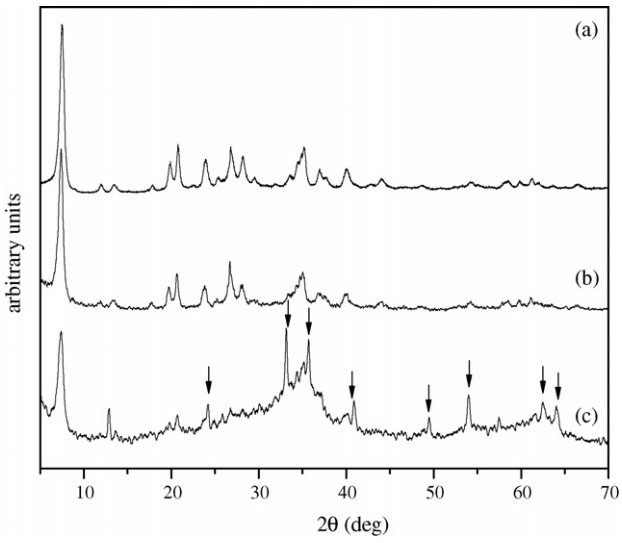

Fig. 2. XRD powder patterns corresponding to sepiolite (a), α-Fe_2O_3/sepiolite S10 (b), α-Fe_2O_3/sepiolite S47 (arrows indicate α-Fe_2O_3 peaks) (c).

ciated by hydrogen bonding to the structure and coordinated water molecules[25] which are bonded to Mg^{2+} ions located at the edges of octahedral sheets. The loss of these coordinated water molecules causes the folding of the structure forming small iron

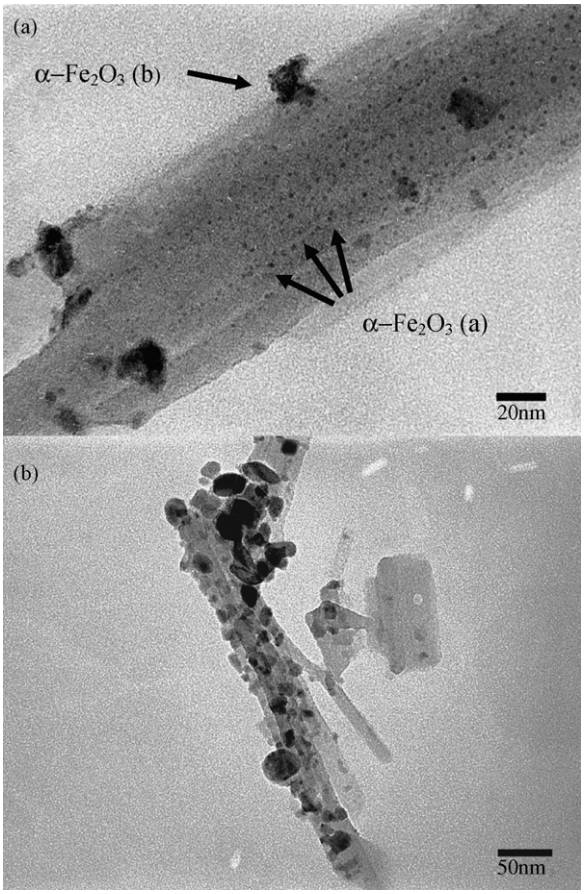

Fig. 3. TEM micrographs corresponding to S10 (a) (inset: α-Fe_2O_3 into the edge of the superficial octahedral layer (a) and deposited on the surface (b)) and S47(b).

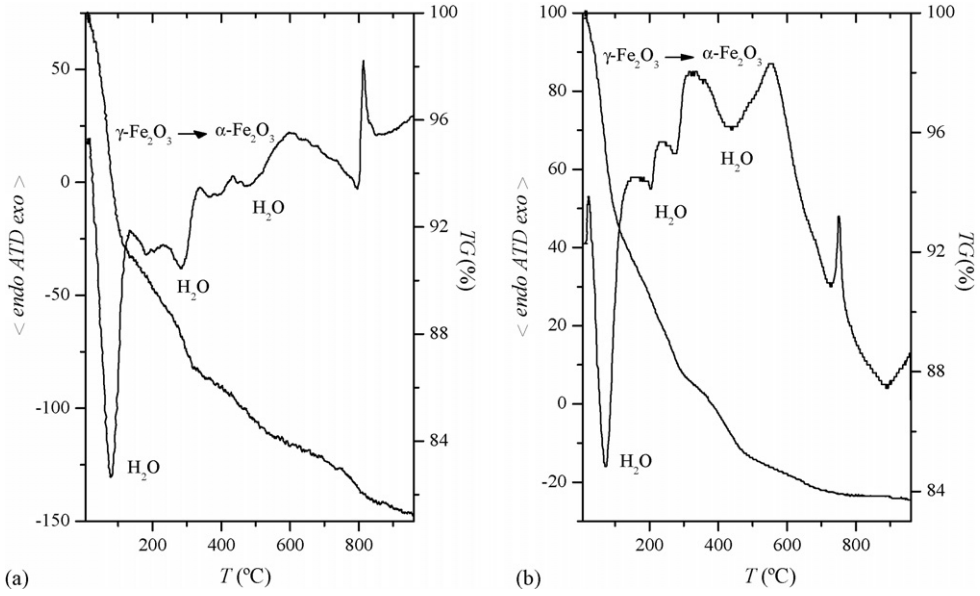

Fig. 4. ATD/TG in air atmosphere of 10 wt.% α-Fe_2O_3 (a) and 47 wt.% α-Fe_2O_3 (b) substituted sepiolite.

oxide nanoparticles. As a result, the channels of the sepiolite structure collapse avoiding any coalescence process. In Fig. 4b, the S47 sample shows two exothermic peaks at 240 and 338 °C corresponding to the maghemite to hematite transition.

Although the sepiolite can lose and recover some zeolitic water, once the dehydration corresponding to coordinated water takes place, the structural change is irreversible and as a consequence the specific surface reduces. Areas for S10 and S47 samples which were found to be 338 and 203 m^2/g at ambient temperature, decreased to 118 and 57 m^2/g, respectively, after heating at 500 °C for 2 h.

Mercury porosimetry measurements were performed on three 0.6 g pellets of each composition heated at 520 °C for 1 h (Fig. 5). Mean pore radius was 7×10^{-3}, 1×10^{-2} and 6×10^{-3} μm, while open porosity was about 48%, 43.1% and 47%, respectively, for the pure sepiolite, S10 and S47 samples. As a result, α-Fe_2O_3 additions to sepiolite did not seem to strongly modify total porosity and mean pore radius.

The nanoparticle size and the morphology of samples were studied by TEM. As can be observed in Fig. 3a, the S10 sample presents iron oxide nanoparticles adsorbed along the sepiolite structure and a few amount, deposited on its surface, with an average size of 3 and 8 nm, respectively. In the case of the S47 sample (Fig. 3b), the amount of iron oxide is so high that sepiolite particles appear partially covered by α-Fe_2O_3 large nanoparticles (25 nm).

Once the sensors were mounted in the humidity chamber under a dehydrated flow, the measured tension died down, cor-

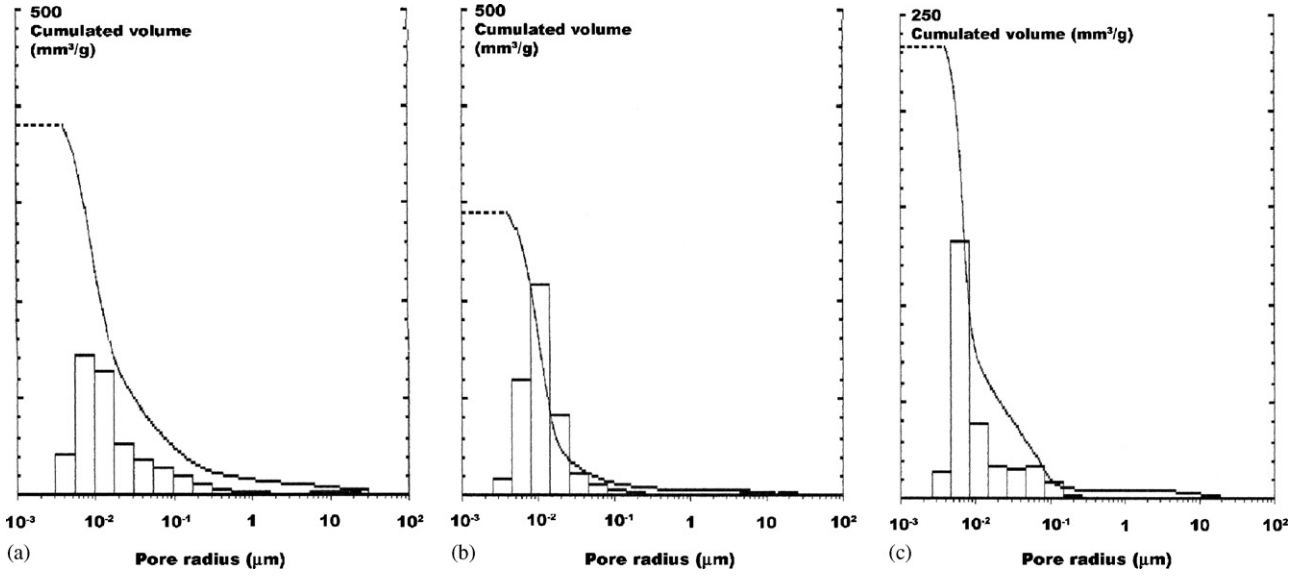

Fig. 5. Mercury porosimetry measurements for pure sepiolite (a), S10 (b) and S47 samples (c).

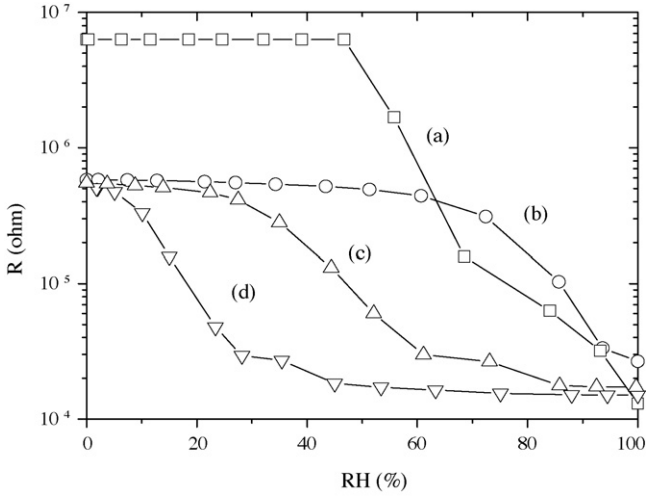

Fig. 6. Variation of the resistance for hematite sample doped with sodium (a), sepiolite (b), S10 (c) and S47 (d) in function of the RH at 30 °C.

responding to a resistance increase because of the hydroxyl groups desorption and the measurements were performed when the monitored V_{DC} became stable. The measurements of the resistance at different RH atmospheres were performed with a dead time, chosen in an arbitrary mode, of 2 min after the RH switch happened. For the sake of comparison, a screen printed hematite sample doped with sodium was analyzed[19] (Fig. 6). All the pellets, including that of pure sepiolite, have a smaller resistance (<1 MΩ) than that of the thick hematite film (≈6 MΩ) (Fig. 6a). The resistance of all the investigated samples died down with increasing RH values: from 60% to 98% for pure sepiolite, from 15% to 70% for S10 and from 5% to 40% for S47 pellets, respectively. These results are very interesting, because they show that the water condensation in the microporosity of the sepiolite pores is governed by hematite additions and the sensor response can be adjusted by varying hematite content. This is also in agreement with the Kelvin equation (3) where the sensing characteristic of an ionic-type humidity sensor is mainly determined by capillary condensation of water in all cylindrical pores, with one end closed, having radii up to the Kelvin radius given by[26]:

$$\ln\left(\frac{P_s}{P}\right) = -\frac{2\gamma M}{\rho RTr} \quad (3)$$

where P and P_s are water vapour pressures in the surrounding environment and at saturation, respectively. M, γ and ρ are the molecular weight, surface tension and density of water, respectively. Because the hematite nanoparticles overlap sepiolite grains, pores of minor dimensions (<1 nm in pellet S47), were first filled with condensed water leading to impedance variations for lower relative humidity values. The exact role of α-Fe_2O_3 additions has to be understood, for example by substituting it by another oxide (γ-Fe_2O_3, for example).

On the other hand, two additional humidity tests were carried out with the aim of evaluating the effect of hematite concentration on the resistance of the sensor as a function of the time. Firstly, the resistances values were measured after 1, 3, 5, 10, 15 and 30 min at the corresponding relative humidity step (Fig. 7). As results, S10 and S47 samples presented huge resistance variations between 5–55% and 5–20% of RH respectively and a very fast response time even after 1 min of measurement (Fig. 7). In the second series of tests, the RH was varied from 0% to 80% by alternating cycles with different steps during 2.5 days. As can be seen in Fig. 8, the response of S10 and S47 samples is so fast that it just needed 3 min to detect a variation from 0% to 80% of RH. Moreover, in this figure the resistance level corresponding to 0% RH is recovered quickly in both samples, so that no hysteresis processes are present.

The fact that α-Fe_2O_3 particles have nanometer size and appear monodisperse, plays an important role in the ability of the adsorbents as humidity controller due to their large specific surface area. According to the results, sepiolite retains water vapour in air at high RH and reacts by large variations in the amount adsorbed, whereas this variation occurs for iron oxide nanoparticles at low-medium RH, as a function of the iron oxide concentration. In this way, a mixture of different iron oxide concentrations on sepiolite produce differences in the variation of the resistance and widen the range of the application of sepiolite as humidity controller.

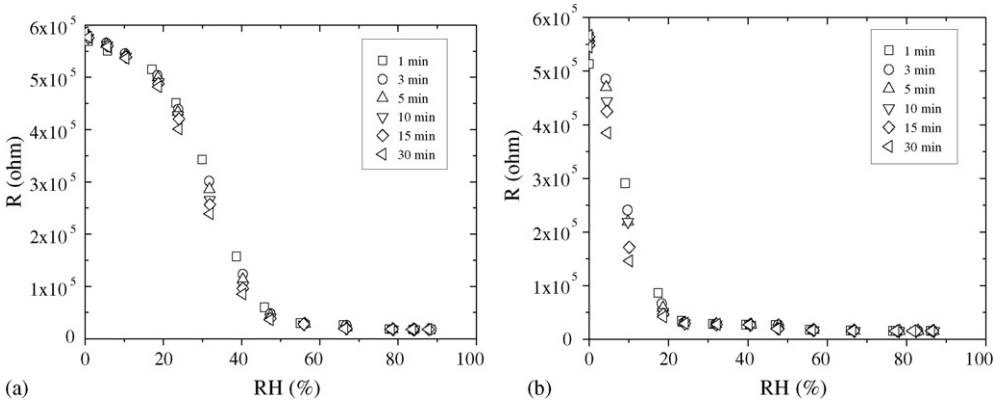

Fig. 7. Resistance of the S10 (a) and S47 (b) samples after 1, 3, 5, 10, 15 and 30 min in function of RH.

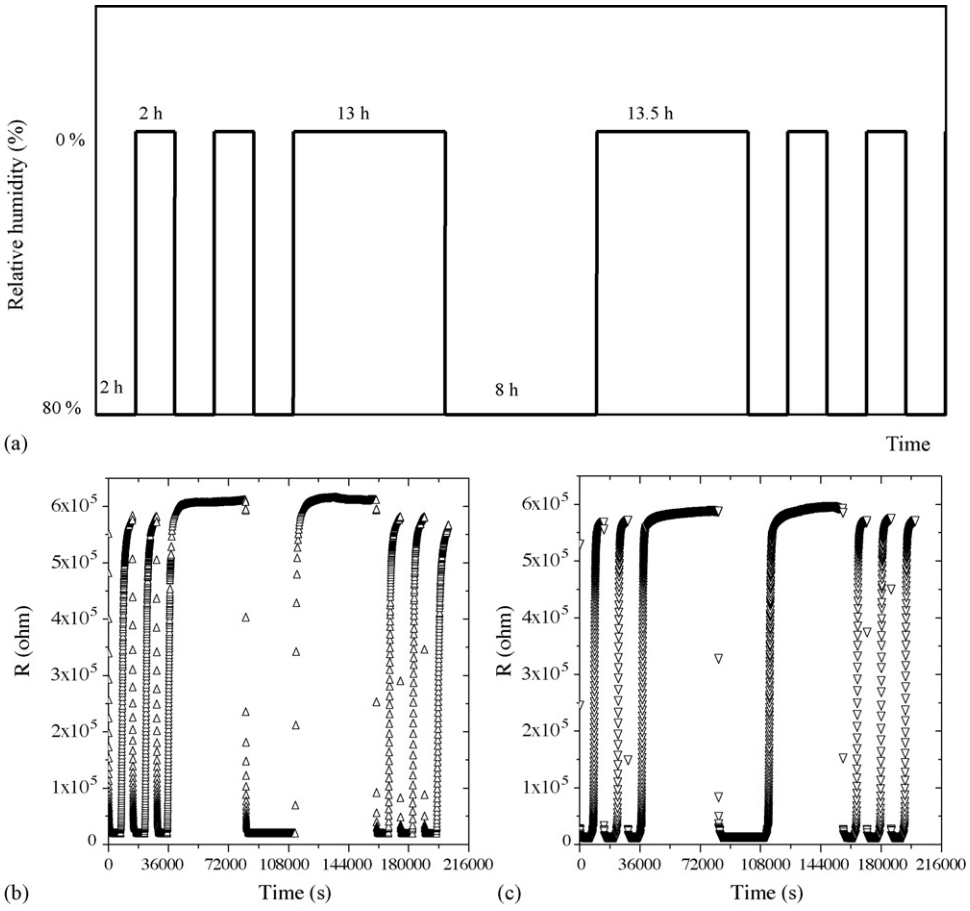

Fig. 8. Alternating cycles of 0% and 80% RH (a) and variation of the resistance in function of the alternating cycles for S10 (b) and S47 (c) samples.

4. Conclusions

Hematite monodispersed nanoparticles have been obtained on sepiolite following a simple low cost wet chemical route. The fact that these nanoparticles appear supported on an inert matrix, makes it possible to avoid manipulation, agglomeration and harmful character that pure nanoparticles usually have. On the other hand, "in situ" precipitation of nanoparticles into one porous matrix notably enlarges the sensibility of these materials as a function of the RH with regard to conventional materials obtained by infiltrating silica. In this sense, a mixture of different iron oxide concentration into sepiolite can be used in a large range of relative humidity (5–98%) as humidity sensor.

According to the results, we can conclude that stable hematite nanoparticles can be easily obtained and scaled-up to produce large amounts of commercial nanoparticles (tonnes) embedded into sepiolite.

Acknowledgements

The Spanish Ministry of Education and Science has supported this research under projects MAT2003-04199-C02 and PTR1995-0832-OP. A.E.C. thanks financial support of the I3P grant by CSIC and European Social Fund (ESF).

References

1. Di Francia, G., Castaldo, A., Massera, E., Nasti, I., Quercia, L. and Rea, I., A very sensitive porous silicon based humidity sensor. *Sens. Actuators B*, 2005, **111–112**, 135–139.
2. Patissier, B., Humidity sensors for automotive, appliances and consumer applications. *Sens. Actuators B*, 1999, **59**, 231–234.
3. Zhang, Y., Yu, K., Ouyang, S., Luo, L., Hu, H., Zhang, Q. *et al.*, Detection of humidity based on quartzcrystal microbalance coated with ZnO nanostructure films. *Physica B*, 2005, **368**, 94–99.
4. Adhikari, B. and Majumdar, S., Polymers in sensor applications. *Progr. Polym. Sci.*, 2004, **29**, 699–766.
5. Laville, C., Delétage, J. Y. and Pellet, C., Humidity sensors for a pulmonary function diagnostic microsystem. *Sens. Actuators B*, 2001, **76**, 304–309.
6. Cunningham, M. J., Development and performance of a small relative humidity sensor for indoor microclimate measurements. *Build. Environ.*, 1999, **34**, 349–352.
7. Wang, C. T. and Wu, C. L., Electrical sensing properties of silica aerogel thin films to humidity. *Thin Solid Films*, 2006, **496**, 658–664.
8. Greenblatt, M. and Feng, S., Proton conducting solid electrolytes for high temperature humidity sensing. In *Proceedings of the Materials Research Society Symposium, Vol. 293*, 1993, pp. 283–294.
9. Park, J. H. and Park, S. J., Effect of V_2O_5 on the electrical-properties of TiO_2–V_2O_5 humidity sensors. *J. Mater. Sci.*, 1994, **5**, 300–304.
10. Chou, K. S., Lee, T. K. and Liu, F. J., Sensing mechanism of a porous ceramic as humidity sensor. *Sens. Actuators B*, 1999, **56**, 106–111.
11. Bearzotti, A., Bertolo, J. M., Innocenzi, P., Falcaro, P. and Traversa, E., Humidity sensors based on mesoporous silica thin films synthesized by block copolymers. *J. Eur. Ceram. Soc.*, 2004, **24**, 1969–1972.

12. Esteban-Cubillo, A., Díaz, C., Fernández, A., Díaz, L. A., Pecharromán, C., Torrecillas, R. *et al.*, Silver nanoparticles supported on α-, η- and δ-alumina. *J. Eur. Ceram. Soc.*, 2006, **26**, 1–7.
13. McCafferty, E. and Zettlemoyer, A. C., Adsorption of water vapor on alpha-Fe_2O_3. *Discuss. Faraday Soc.*, 1971, **52**, 239–255.
14. Neri, G., Bonavita, A., Galvagno, S., Pace, C., Patané, S. and Arena, A., Humidity sensing properties of Li-iron oxide based-thin films. *Sens. Actuators B*, 2001, **73**, 89–94.
15. Neri, G., Bonavita, A., Milone, C., Pistone, A. and Galvagno, S., Gold promotes Li-Fe_2O_3 thin films for humidity sensors. *Sens. Actuators B*, 2003, **92**, 326–330.
16. Zucco, M., Negro, A., Montanaro, L., Humidity sensor, European Patent 1293770 A2, 2002.
17. Pelino, M., Cantalini, C., Sun, H. T. and Faccio, M., Silica effect on alpha-Fe_2O_3 humidity sensor. *Sens. Actuators B*, 1998, **46**, 186–193.
18. Brauner, K. and Preisinger, A., Struktur und Enstehung des Sepioliths. *Tschermarks Mineral. Petrogr. Mitt.*, 1956, **6**, 120–140.
19. Tulliani, J. M. and Bonville, P., Influence of the dopants on the electrical resistance of hematite-based humidity sensors. *Ceram. Int.*, 2004, **31**, 507–514.
20. Sabah, E., Turan, M. and Celik, M. S., Adsorption mechanism of cationic surfactants onto acid- and heat-activated sepiolites. *Water Res.*, 2002, **36**, 3957.
21. Jiménez-López, A., López-González, J. deD., Ramírez-Sáez, A., Rodríguez-Reinoso, F., Valenzuela-Calahorro, C. and Zurita-Herrera, L., Evolution of surface area in a sepiolite as a function of acid and heat treatments. *Clay Miner.*, 1978, **13**, 375.
22. González, L., Ibarra, L. M., Rodríguez, A., Moya, J. S. and Valle, F. J., Fibrous silica gel obtained from sepiolite by HCl attack. *Clay Miner.*, 1984, **19**, 93.
23. Pourbaix, M., *Atlas electrochemical equilibria in aqueous solutions*. National Association of Corrosion Engineers, Texas, 1974.
24. Preisinger, A., X-ray study of the structure of sepiolite. In *Proceedings of the sixth conference on clays and clay minerals*, 1959, p. 61.
25. Frost, R. L. and Ding, Z., Controlled rate thermal analysis and differential scanning calorimetry of sepiolites and palygorskites. *Thermochim. Acta*, 2003, **397**, 119.
26. Yamazoe, N. and Shimizu, Y., Humidity sensor: principles and applications. *Sens. Actuators*, 1986, **10**, 379–398.